

# A holey-structured metamaterial for acoustic deep-subwavelength imaging

J. Zhu<sup>1†</sup>, J. Christensen<sup>2†</sup>, J. Jung<sup>2,3</sup>, L. Martin-Moreno<sup>4</sup>, X. Yin<sup>1</sup>, L. Fok<sup>1</sup>, X. Zhang<sup>1\*</sup> and F. J. Garcia-Vidal<sup>2\*</sup>

**For classical waves such as light or sound, diffraction sets a natural limit on how finely the details of an object can be recorded on its image. Recently, various optical superlenses based on the metamaterials concept have shown the possibility of overcoming the diffraction limit<sup>1–7</sup>. Similar two-dimensional (2D) acoustic hyperlens designs have also been explored<sup>8–10</sup>. Here we demonstrate a 3D holey-structured metamaterial that achieves acoustic imaging down to a feature size of  $\lambda/50$ . The evanescent field components of a subwavelength object are efficiently transmitted through the structure as a result of their strong coupling with Fabry–Pérot resonances inside the holey plate. This capability of acoustic imaging at a very deep-subwavelength scale may open the door for a broad range of applications, including medical ultrasonography, underwater sonar and ultrasonic non-destructive evaluation.**

The design and experimental realization of man-made electromagnetic<sup>11–13</sup> and sonic<sup>14–16</sup> metamaterials have created many fascinating avenues in optics and acoustics research in recent years. Among these new possibilities, the discovery that a thin slab of artificially microstructured metamaterial can act as a perfect lens<sup>1</sup> and restore all the evanescent components of a near-field image, has had a profound impact on optical subwavelength imaging, that is, in the search to overcome the so-called diffraction limit. To overcome the same limitation in acoustic imaging, previous studies have described strategies such as time-reversal techniques<sup>17,18</sup> and the use of Bragg-scattering in phononic crystals<sup>19–26</sup>. In the time-reversal approach, the inherently complex set-up reduces its robustness, whereas for lenses based on phononic crystals, the lattice constant must be of the same order as the acoustic wavelength, which results in an imaging resolution that is limited by diffraction. Recently, 2D acoustic lenses based on metamaterials have been explored<sup>8–10</sup>. To the best of our knowledge, the best resolution achieved with this type of 2D lens is  $\lambda/7$  (ref. 12).

Here we report a new class of 3D acoustic metamaterials that operate as near-field imaging devices. The basic structure, which consists of a rigid block (impenetrable for sound waves) of thickness  $h$ , perforated with deep-subwavelength square holes of side  $a$  forming a periodic array with lattice parameter  $\Lambda$  (Fig. 1a), is surrounded by air. Previous work suggests that it may be difficult to conduct 3D optical subwavelength imaging with holey metal structures because the holes must be filled with a material having a very high dielectric constant<sup>27</sup>. However, because of the absence of a cutoff frequency in the acoustic case, propagation of acoustic waves inside deep-subwavelength-sized apertures is possible and

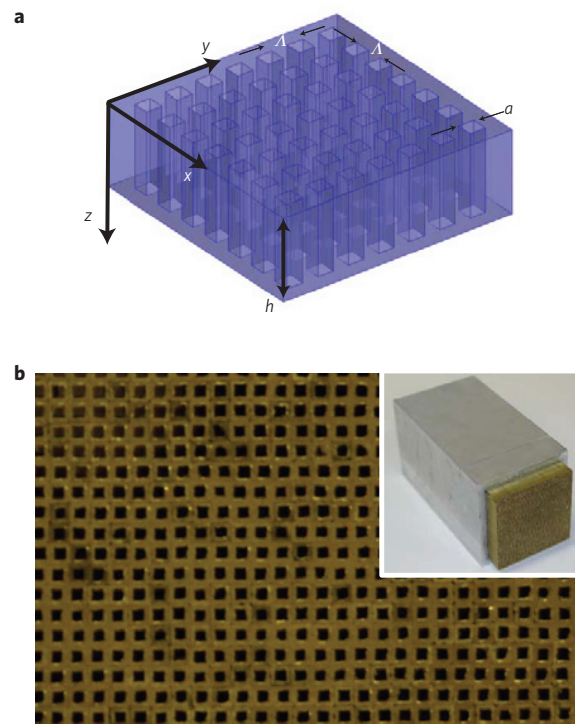


**Figure 1 | Holey-structured metamaterial for deep-subwavelength acoustic imaging. a**, Schematic of the square array of holes drilled in a rigid block. The period of the array is  $\Lambda$ , the side of the square holes is  $a$  and the plate thickness is  $h$ . **b**, For the experimental realization, 1,600 ( $40 \times 40$ ) square brass alloy tubes are used, with the geometrical parameters of the sample chosen to be:  $a = 0.79$  mm,  $\Lambda = 1.58$  mm and  $h = 158$  mm. All the tubes are fitted in parallel into a 4-inch-wide square aluminium tube and clamped firmly together. Superglue is applied between the tubes to prevent any movement or vibration under pressure.

can lead to the formation of Fabry–Pérot transmission resonances. For subwavelength imaging, it is worth noting that, as we will show below, these Fabry–Pérot resonant modes can be excited by the evanescent waves scattered from the object. As a result, information carried by the evanescent waves is successfully transmitted through this holey metamaterial. More importantly, those evanescent waves contain much larger wave vectors than that of the propagating

<sup>1</sup>Nanoscale Science and Engineering Center (SINAM), 3112 Etcheverry Hall, University of California, Berkeley, California 94720, USA, <sup>2</sup>Departamento de Física Teórica de la Materia Condensada, Universidad Autónoma de Madrid, E-28049 Madrid, Spain, <sup>3</sup>Department of Physics and Nanotechnology, Aalborg University, Skjernvej 4A, DK-9220 Aalborg Øst, Denmark, <sup>4</sup>Instituto de Ciencia de Materiales de Aragón (ICMA) and Departamento de Física de la Materia Condensada, CSIC-Universidad de Zaragoza, E-50009, Zaragoza, Spain. <sup>†</sup>These authors contributed equally to this work.

\*e-mail: xiang@berkeley.edu; fj.garcia@uam.es.

wave inside the holes and, therefore, contribute to restoring an image with a feature size far below the diffraction limit. The ability of this holey metamaterial to resolve subwavelength features also depends on the geometrical parameters of the structure. It has been shown for electromagnetic waves that the imaging resolution of holey metal films is determined by the period of the array<sup>27</sup>, which can be made much smaller than the operating wavelength. We have found that the same behaviour occurs for acoustic waves.

The capability of this holey structure to resolve all the spatial information of an acoustic image can be explained within the effective medium approach. It can be shown (see Supplementary Information for details) that, in the limit in which all diffraction effects can be safely neglected and the transmission process is dominated by the fundamental propagating mode inside the holes ( $\lambda \gg \Lambda, a$ ), the zero-order transmission coefficient for an acoustic plane wave of parallel momentum  $k_{\parallel} = \sqrt{k_x^2 + k_y^2}$  can be written as:

$$t(\lambda, k_{\parallel}) = \frac{4|S_{00}|^2 Y \exp(iq_z h)}{(1 + Y|S_{00}|^2)^2 - (1 - Y|S_{00}|^2)^2 \exp(2iq_z h)} \quad (1)$$

where  $q_z = k_0 = 2\pi/\lambda$  is the propagation constant of the above-mentioned fundamental waveguide mode,  $S_{00} = a/\Lambda$  and  $Y = k_0/\sqrt{k_0^2 - k_{\parallel}^2}$ . The important point is that, at the resonance condition for standing-wave excitation ( $q_z h = m\pi$ , with  $m$  an integer), the transmission coefficient has unity modulus for all parallel momenta, including evanescent waves. This result suggests that, if an object is placed at the input side of the holey plate, its acoustical image can be perfectly transferred to the output side. The dependence of the zero-order transmission coefficient versus parallel momentum and frequency, as rendered in Fig. 2, clearly supports this point. At the Fabry–Pérot resonant frequencies ( $m = 1-4$ ), the dispersion curves of the Fabry–Pérot modes are very flat over a wide range of wave vectors, both in the propagating and evanescent regions of the  $k$ -space, and their associated transmission coefficients have unity modulus. Therefore, most of the parallel momentum can be carried over and used in imaging. It can be shown that this holey-structured metamaterial behaves effectively as an anisotropic homogeneous slab. As the dispersion of the fundamental mode inside the holes is unaffected by parallel momentum,  $\rho_{\text{eff}}^z = 1/K_{\text{eff}}^z = \infty$ . In the parallel directions ( $x$  and  $y$ ), the metamaterial is characterized by a mass density equal to  $\rho_{\text{eff}}^x = \rho_{\text{eff}}^y = \rho_{\text{eff}} = \rho_{\text{air}} \Lambda^2/a^2$  and a bulk modulus  $K_{\text{eff}}^x = K_{\text{eff}}^y = K_{\text{eff}} = K_{\text{air}} \Lambda^2/a^2$ , in such a way that the velocity of sound is equal to that of air (see Supplementary Information for details). Different from the perfect lens presented in ref. 1, this holey metamaterial presents an infinitely anisotropic structure that allows wave propagation in the direction perpendicular to the interfaces, so the evanescent fields are not amplified. The physics behind the behaviour of the holey-structured metamaterial is similar to the so-called canalization phenomenon<sup>28</sup>, which has been used for the faithful transfer of a near-field electromagnetic subwavelength image from the input to output surface of a system that acts as a kind of subwavelength endoscope. Examples of this type of phenomenon have been reported before for electromagnetic waves<sup>29-33</sup>. A metamaterial made of Swiss-roll wires was able to transfer an input magnetic field pattern to the output face with little loss of intensity<sup>33</sup>. It has also been shown that a periodic array of long wires can act as an electromagnetic subwavelength endoscope<sup>30-33</sup>. However, the acoustic version of such a structure (a period array of wires made of a rigid material) is not able to transfer the subwavelength details of an object (see Supplementary Information for details). This result neatly illustrates the differences between electromagnetic and acoustic waves when they propagate through structured materials.

To corroborate the subwavelength imaging capabilities of a holey-structured metamaterial, we have carried out full 3D numerical calculations using a modal expansion technique that

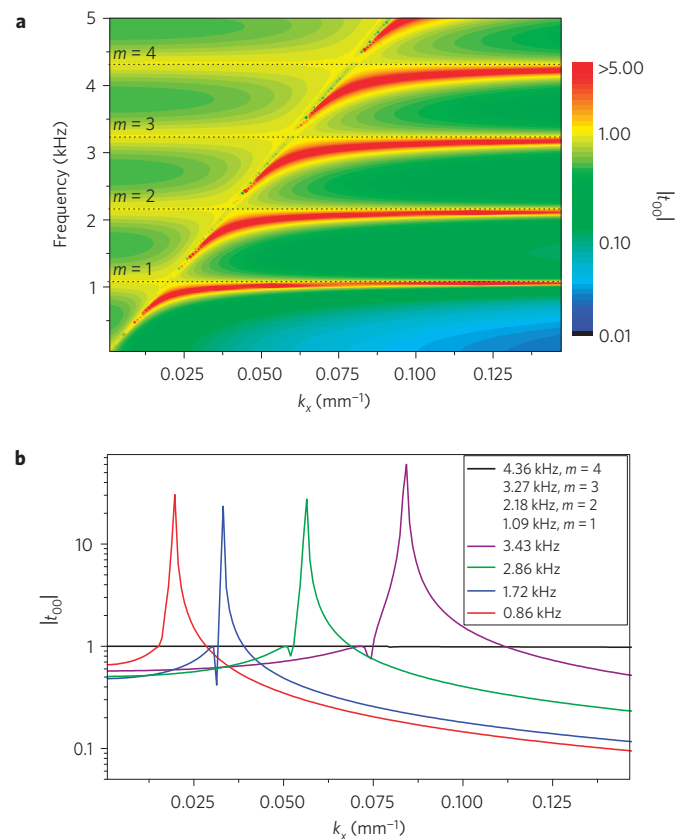


**Figure 2 | Dispersion relations.** **a**, Simulated modulus of the zero-order transmission coefficient versus parallel momentum ( $x$  axis) and frequency ( $y$  axis) on a logarithmic scale. At the Fabry–Pérot resonances ( $m = 1, 2, 3, 4$ ), the modulus of the transmission coefficient is one. The flatness of the dispersion curves can clearly be observed. The simulations were done for holey metamaterial in air. Notice that the edge of the first Brillouin zone would appear at  $k_x = \pi/\Lambda \approx 2 \text{ mm}^{-1}$ . **b**, Simulated modulus of the zero-order transmission coefficient evaluated at eight different frequencies: the first four correspond to the four lowest Fabry–Pérot resonant frequencies and the remaining four to frequencies intermediate to these.

contains as many diffraction orders as needed for convergence. As the image source, two subwavelength square dots are perforated in a zero-thickness screen (see Fig. 3a), placed on top of the holey plate and excited by an acoustic plane wave. The operating frequency and wavelength are chosen to be  $f = 2.18 \text{ kHz}$  and  $\lambda = h = 158 \text{ mm}$ , which corresponds to mode  $m = 2$  for the standing-wave resonance condition. The size of the dots is  $w = 7.9 \text{ mm}$  ( $\lambda/20$ ) with a centre-to-centre distance  $s = 11.85 \text{ mm}$  ( $\lambda/13.3$ ). As shown in Fig. 3b, if we simulate the image plane at one lattice constant  $\Lambda$  from the exact output plane, a faithful image of the two dots can be obtained, as both equation (1) and the simulations shown in Fig. 2 predict. This confirms that a holey-structured metamaterial behaves as a near-field acoustic imaging device able to operate on a very deep-subwavelength scale.

We have conducted experiments in air to test this hypothesis. As a source object, a thin brass plate perforated with two subwavelength square holes is placed immediately in front of the device, such that the scattered evanescent waves from the object can be coupled into the metamaterial. A speaker, 20 mm in diameter, producing continuous sinusoidal waves is placed 20 cm before the source object. A microphone is attached to a 3D scanning system and used to measure the acoustic field distribution on the output side. Sound-absorbing material is packed around the scanning area

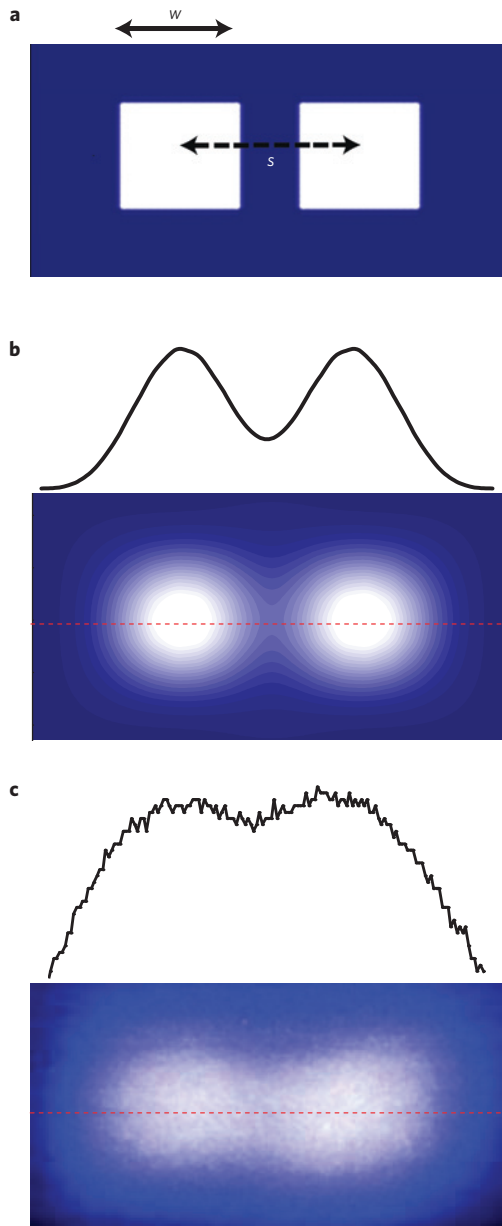


**Figure 3 | Simulation and experimental images of two square dots.**

**a**, The image source is composed of two square dots (side  $w = 7.9$  mm) with a centre-to-centre distance  $s = 11.85$  mm, perforated in a zero-thickness screen that is placed at the input side. The operating frequency is chosen to be 2.18 kHz, which corresponds to  $\lambda = h = 158$  mm and  $m = 2$  in Fig. 2 for the standing-wave resonance condition. **b**, Simulation result of the spatial pressure field and the distribution along the cross-section indicated by the red dashed line for an image plane at a distance  $\Lambda = 1.58$  mm from the exact output plane. **c**, Experimentally measured pressure field in the same conditions as in **b**.

to prevent external noise. The image measured at  $\Lambda = 1.58$  mm from the output plane shows an acoustic field pattern with two bright dots and a clear gap between them (Fig. 3c), in good agreement with the numerical simulations. Our experiments also show that this holey metamaterial functions at other frequencies that satisfy that standing-wave resonance condition (see Supplementary Information for details).

In the panels of Fig. 4, we show images of an object shaped like the letter 'E' (Fig. 4a). It can be seen that a linewidth of 3.18 mm ( $\lambda/50$ ) can be clearly resolved (Fig. 4b), also in good

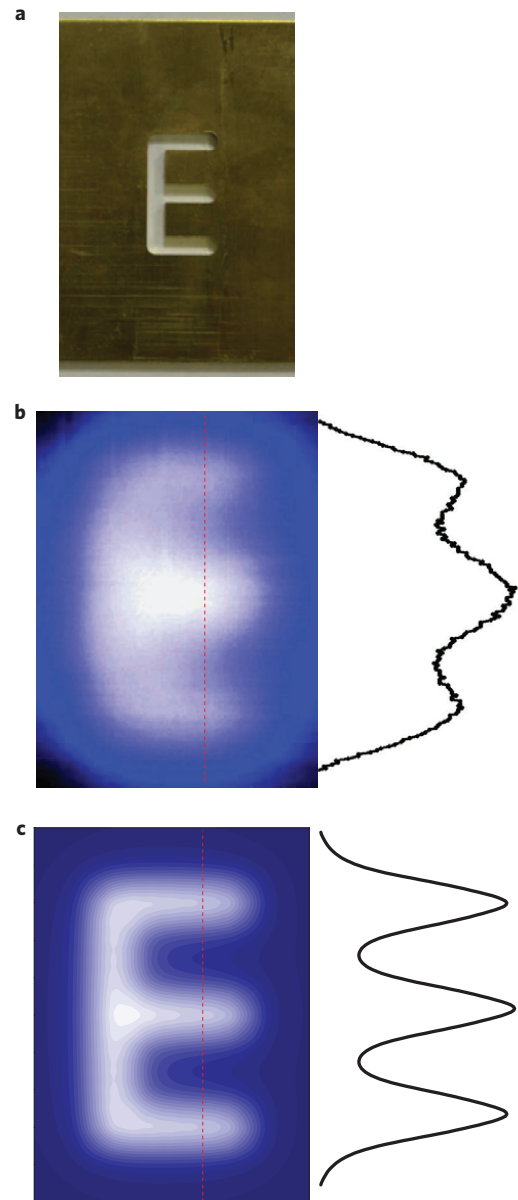


**Figure 4 | Simulation and experimental imaging of deep-subwavelength-sized letter E.**

**a**, Imaging object: letter 'E' with a linewidth 3.18 mm perforated in an ultrathin brass plate. **b**, Measured image of letter 'E', obtained at a distance  $\Lambda = 1.58$  mm from the output plane, and the acoustic field distribution along the cross-section indicated by the red dashed line. The operating frequency is 2.18 kHz ( $\lambda = 158$  mm). A  $\lambda/50$  linewidth of the object can still be observed. **c**, Simulated image of letter 'E', obtained at a distance  $\Lambda = 1.58$  mm from the output plane, and the acoustic field distribution along the cross-section indicated by the red dashed line.

agreement with the simulation (Fig. 4c). Despite mild blurring at some fringe points, the shape of the whole pattern remains intact at the imaging plane; subwavelength details at the line edges and corners are also well produced. Therefore, we have demonstrated that this holey metamaterial can faithfully project an image with deep-subwavelength details ( $\lambda/50$ ). As mentioned above, the effective transmission of such a subwavelength image relies on the Fabry–Pérot resonances excited inside the holey structure. In such circumstances, the evanescent field components with large wave vectors scattered from the object are strongly coupled to the transmission resonant modes, thus being carried over to the output side to form a very sharp image. However, if

the operating wavelength is detuned from the resonance condition the image quality deteriorates rapidly, and the whole image is eventually reduced to a blurred spot owing to the loss of the deep-subwavelength details of the object. In addition, information carried by the large wave vectors is also progressively lost when the image plane moves away from the exit surface of this metamaterial (see Supplementary Information for details). Although the ultimate feature resolution is theoretically predicted to be at the scale of the lattice constant ( $\lambda$ ) of the metamaterial, which is about  $\lambda/100$ , the size of the microphones (3.2 mm in diameter) sets a practical limit for the feature size of  $\lambda/50$  in our experimental set-up. It is worth noting that the acoustical properties of holey plates have recently been studied<sup>34–37</sup>, mainly in connection with the phenomenon of extraordinary acoustical transmission. Two different types of transmission resonance exist in holey plates. One is associated with the excitation of acoustic surface waves with spectral locations that disperse strongly with parallel momentum, where the resonant wavelength appears close to the period of the hole array. The second class of transmission resonance is the non-dispersive Fabry–Pérot modes that have been discussed in detail in our work. As we have shown, the resonant wavelengths of the Fabry–Pérot modes are mainly controlled by the thickness of the perforated plate. In our study, the holey plates are within the metamaterial limit, in which the operating wavelength is much larger than the period of the array. Therefore, Fabry–Pérot resonances dominate the transmission process and acoustic surface waves play a negligible role.

Our experimental results confirm that a holey-structured metamaterial can act as a nearly perfect imaging device by reproducing the deep-subwavelength information of an object. This device operates at a discrete set of resonant frequencies, corresponding to the Fabry–Pérot modes of the system. Experimentally demonstrated imaging with a feature size of  $\lambda/50$  shows the resolving power of our holey metamaterial lies well below the diffraction limit. Scaling down the geometrical parameters should further enhance the performance of the device at higher frequencies. Apart from being of fundamental interest, holey metamaterials could be used to improve medical ultrasonic imaging for scanning and diagnostic purposes, for the non-destructive detection of cracks in alloy materials, as well as in other applications.

Received 4 March 2010; accepted 3 September 2010;  
published online 7 November 2010

## References

- Pendry, J. B. Negative refraction makes a perfect lens. *Phys. Rev. Lett.* **85**, 3966–3969 (2000).
- Smith, D. R., Pendry, J. B. & Wiltshire, M. C. K. Metamaterials and negative refractive index. *Science* **305**, 788–792 (2004).
- Soukoulis, C. M., Linden, S. & Wegener, M. Negative refractive index at optical wavelengths. *Science* **315**, 47–49 (2007).
- Fang, N., Lee, H., Sun, C. & Zhang, X. Sub-diffraction-limited optical imaging with a silver superlens. *Science* **308**, 534–537 (2005).
- Taubner, T., Korobkin, D., Urzhumov, Y., Shvets, G. & Hillenbrand, R. Near-field microscopy through a SiC superlens. *Science* **313**, 1595 (2006).
- Liu, Z., Lee, H., Xiong, Y., Sun, C. & Zhang, X. Far-field optical hyperlens magnifying sub-diffraction-limited objects. *Science* **315**, 1686 (2007).
- Liu, Z. *et al.* Far-field optical superlens. *Nano Lett.* **7**, 403–408 (2007).
- Guenneau, S., Movchan, A., Pétursson, G. & Ramakrishna, S. A. Acoustic meta-materials for sound focussing and confinement. *New J. Phys.* **9**, 1367–2630 (2007).
- Ao, X. & Chan, C. T. Far-field image magnification for acoustic waves using anisotropic acoustic metamaterials. *Phys. Rev. E* **77**, 025601(R) (2008).
- Li, J., Fok, L., Yin, X., Bartal, G. & Zhang, X. Experimental demonstration of an acoustic magnifying hyperlens. *Nature Mater.* **8**, 931–934 (2009).
- Pendry, J. B., Holden, A. J., Robbins, D. J. & Stewart, W. J. Magnetism from conductors and enhanced nonlinear phenomena. *IEEE Trans. Microw. Theory Tech.* **47**, 2075–2084 (1999).
- Smith, D. R., Padilla, W. J., Vier, D. C., Nemat-Nasser, S. C. & Schultz, S. Composite medium with simultaneously negative permeability and permittivity. *Phys. Rev. Lett.* **84**, 4184–4187 (2000).

- Shalae, V. M. Optical negative-index metamaterials. *Nature Photon.* **1**, 41–48 (2006).
- Liu, Z. *et al.* Locally resonant sonic materials. *Science* **289**, 1734–1736 (2000).
- Fang, N. *et al.* Ultrasonic metamaterials with negative modulus. *Nature Mater.* **5**, 452–456 (2006).
- Zhang, S., Yin, L. & Fang, N. Focusing ultrasound with an acoustic metamaterial network. *Phys. Rev. Lett.* **102**, 194301 (2009).
- de Rosny, J. & Fink, M. Overcoming the diffraction limit in wave physics using a time-reversal mirror and a novel acoustic sink. *Phys. Rev. Lett.* **89**, 124301 (2002).
- Lerosey, G., de Rosny, J., Tourin, A. & Fink, M. Focusing beyond the diffraction limit with far-field time reversal. *Science* **315**, 1120–1122 (2007).
- Yang, S. *et al.* Focusing of sound in a 3D phononic crystal. *Phys. Rev. Lett.* **93**, 024301 (2004).
- Zhang, X. D. & Liu, Z. Y. Negative refraction of acoustic waves in two-dimensional phononic crystals. *Appl. Phys. Lett.* **85**, 341–343 (2004).
- Sukhovich, A., Jing, L. & Page, J. H. Negative refraction and focusing of ultrasound in two-dimensional phononic crystals. *Phys. Rev. B* **77**, 014301 (2008).
- Sukhovich, A. *et al.* Experimental and theoretical evidence for subwavelength imaging in phononic crystals. *Phys. Rev. Lett.* **102**, 154301 (2009).
- He, Z., Cai, F., Ding, Y. & Liu, Z. Subwavelength imaging of acoustic waves by a canalization mechanism in a two-dimensional phononic crystal. *Appl. Phys. Lett.* **93**, 233503 (2008).
- Cervera, F. *et al.* Refractive acoustic devices for airborne sound. *Phys. Rev. Lett.* **88**, 023902 (2002).
- Yang, S. *et al.* Focusing of sound in a 3D phononic crystal. *Phys. Rev. Lett.* **93**, 024301 (2004).
- Ke, M. *et al.* Flat superlens by using negative refraction in two-dimensional phononic crystals. *Solid State Commun.* **142**, 177–180 (2007).
- Jung, J., Garcia-Vidal, F. J., Martin-Moreno, L. & Pendry, J. B. Holey metal films make perfect endoscopes. *Phys. Rev. B* **79**, 153407 (2009).
- Belov, P. A., Simovski, C. R. & Ikonen, P. Canalization of subwavelength images by electromagnetically induced transparency. *Phys. Rev. B* **71**, 193105 (2005).
- Wiltshire, M. C. K., Hajnal, J., Pendry, J. B., Edwards, D. & Stevens, C. Metamaterial endoscope for magnetic field transfer: Near field imaging with magnetic wires. *Opt. Expr.* **11**, 709–715 (2003).
- Belov, P. A. & Silveirinha, M. G. Resolution of subwavelength transmission devices formed by a wire medium. *Phys. Rev. E* **73**, 056607 (2006).
- Silveirinha, M. G., Belov, P. A. & Simovski, C. R. Ultimate limit of resolution of subwavelength imaging devices formed by metallic rods. *Opt. Lett.* **33**, 1726–1728 (2008).
- Shvets, G., Trendafilov, S., Pendry, J. B. & Sarychev, A. Guiding, focusing, and sensing on the subwavelength scale using metallic wire arrays. *Phys. Rev. Lett.* **99**, 053903 (2007).
- Kawata, S., Ono, A. & Verma, P. Subwavelength colour imaging with a metallic nanolens. *Nature Photon.* **2**, 438–442 (2008).
- Lu, M. *et al.* Extraordinary acoustic transmission through a 1D grating with very narrow apertures. *Phys. Rev. Lett.* **99**, 174301 (2007).
- Christensen, J., Martin-Moreno, L. & Garcia-Vidal, F. J. Theory of resonant acoustic transmission through subwavelength apertures. *Phys. Rev. Lett.* **101**, 014301 (2008).
- Estrada, H. *et al.* Extraordinary sound screening in perforated plates. *Phys. Rev. Lett.* **101**, 084302 (2008).
- Zhou, Y. *et al.* Acoustic surface evanescent wave and its dominant contribution to extraordinary acoustic transmission and collimation of sound. *Phys. Rev. Lett.* **104**, 164301 (2010).

## Acknowledgements

This work has been partially financially supported by the Spanish Ministry of Science under projects MAT2008-06609-C02 and CSD2007-046-Nanolight.es. J.Z. and X.Z. acknowledge support from the US Office of Naval Research (grant number N00014-07-1-0626). We thank M. Nesterov for conducting the finite-element method simulations on wire arrays and holey plates presented in the Supplementary Information.

## Author contributions

F.J.G.-V., J.J. and L.M.-M. developed the idea of using holey films for deep-subwavelength imaging. J.C. and J.Z. devised the acoustic structure. J.Z., X.Y., L.F. and X.Z. designed and carried out the experiments. J.C. conducted the numerical simulations. J.Z., X.Z., L.M.-M. and F.J.G.-V. wrote the manuscript and J.C., J.J., X.Y. and L.F. participated in the revisions. F.J.G.-V. and X.Z. conceived and led the project.

## Additional information

The authors declare no competing financial interests. Supplementary information accompanies this paper on [www.nature.com/naturephysics](http://www.nature.com/naturephysics). Reprints and permissions information is available online at <http://npg.nature.com/reprintsandpermissions>. Correspondence and requests for materials should be addressed to F.J.G.-V.